AGU PUBLICATIONS

Global Biogeochemical Cycles

RESEARCH ARTICLE
10.1002/2016GB005383

Key Points:
- Mesoscale nitrate flux can exceed uptake, convection, and mixing fluxes
- Different scales of variability in nitrate and upwelling may reduce transport
- Nonzero net vertical velocity can bias extrapolation of estimates

Correspondence to:
A. P. Martin,
adrian.martin@noc.ac.uk

Citation:
Pidcock, R. E. M., A. P. Martin, S. C. Painter, J. T. Allen, M. A. Srokosz, A. Forryan, M. Stinchcombe, and D. A. Smeed (2016), Quantifying mesoscale-driven nitrate supply: A case study, *Global Biogeochem. Cycles*, *30*, 1206–1223, doi:10.1002/2016GB005383.

Received 29 JAN 2016
Accepted 7 JUL 2016
Accepted article online 13 JUL 2016
Published online 29 AUG 2016

Quantifying mesoscale-driven nitrate supply: A case study

Rosalind E. M. Pidcock[1,2], Adrian P. Martin[1], Stuart. C. Painter[1], John T. Allen[3], Meric A. Srokosz[1], Alex Forryan[2], Mark Stinchcombe[1], and David A. Smeed[1]

[1]Ocean Biogeochemistry and Ecosystems, National Oceanography Centre, Southampton, UK, [2]Ocean and Earth Sciences, University of Southampton, Waterfront Campus, National Oceanography Centre, Southampton, UK, [3]School of Earth and Environmental Sciences, University of Portsmouth, Portsmouth, UK

Abstract The supply of nitrate to surface waters plays a crucial role in maintaining marine life. Physical processes at the mesoscale (~10–100 km) and smaller scale have been advocated to provide a major fraction of the global supply. While observational studies have focused on well-defined features, such as isolated eddies, the vertical circulation and nutrient supply in a typical 100–200 km square of ocean will involve a turbulent spectrum of interacting, evolving, and decaying features. A crucial step in closing the ocean nitrogen budget is to be able to rank the importance of mesoscale fluxes against other sources of nitrate for surface waters for a representative area of open ocean. While this has been done using models, the vital observational equivalent is still lacking. To illustrate the difficulties that prevent us from putting a global estimate on the significance of the mesoscale observationally, we use data from a cruise in the Iceland Basin where vertical velocity and nitrate observations were made simultaneously at the same high spatial resolution. Local mesoscale nitrate flux is found to be an order of magnitude greater than that due to small-scale vertical mixing and exceeds coincident nitrate uptake rates and estimates of nitrate supply due to winter convection. However, a nonzero net vertical velocity for the region introduces a significant bias in regional estimates of the mesoscale vertical nitrate transport. The need for synopticity means that a more accurate estimate cannot be simply found by using a larger survey area. It is argued that time series, rather than spatial surveys, may be the best means to quantify the contribution of mesoscale processes to the nitrate budget of the surface ocean.

1. Introduction

Quantifying the exchange of nutrients between the surface and deeper ocean is crucial to our understanding of ocean biogeochemical cycling. More specifically, the vertical transport of nitrate is a significant control on the biological carbon pump—the export of organic material, originally fixed by photosynthesis, to the ocean's interior and a significant conduit of carbon dioxide out of the atmosphere.

Early biogeochemical studies, in the oligotrophic western North Atlantic, indicated that the rate of nitrate uptake in surface waters that could be estimated from independent geochemical techniques (~0.5 mol N m^{-2} yr^{-1}) far outweighed the transport of nitrate to the euphotic zone that could be attributed to sources recognized at the time [*Jenkins*, 1988; *Jenkins and Goldman*, 1985; *Jenkins and Wallace*, 1992; *Sarmiento et al*., 1990; *Spitzer and Jenkins*, 1989]. Of the nitrate requirement in this region just 25–30% could be attributed to winter convective overturning [*Michaels et al*., 1994] and the estimated contribution from turbulent mixing at the base of the euphotic zone was also small, at approximately 10% [*Ledwell et al*., 1993, 1998; *Lewis et al*., 1986].

Since then, a substantial and increasing number of numerical modeling and observational studies have indicated that episodic upwelling associated with mesoscale eddies and fronts may provide a significant contribution to balancing this budget of annual nutrient supply [e.g., *Falkowski et al*., 1991; *Jenkins*, 1988; *Klein and Lapeyre*, 2009; *Levy et al*., 2001; *Mahadevan and Archer*, 2000; *McGillicuddy et al*., 1999, 2003; *Woods*, 1988]. However, while the potential for significant contribution by mesoscale (~10–100 km) [*McGillicuddy*, 2016], and submesoscale (~1–10 km) [*Mahadevan*, 2015], processes may be well established, quantitative estimates of the regional contribution of these processes to the nitrate budget vary by an order of magnitude (~0.1 to more than 1.0 mol N m^{-2} yr^{-1}) [e.g., *Falkowski et al*., 1991; *Lapeyre and Klein*, 2006; *Levy et al*., 2001; *Mahadevan and Archer*, 2000; *McGillicuddy et al*., 2003; *McGillicuddy and Robinson*, 1997; *Oschlies*, 2002; *Siegel et al*., 1999]. *McGillicuddy et al*. [2003] directly addressed the question of how significant the

mesoscale transport of nitrate is to nitrogen budgets by using a 0.2° resolution global biogeochemical model. This allowed them to provide a decomposition of the budget at a number of well-studied sites (Bermuda Atlantic Time Series (BATS), North Atlantic Bloom Experiment (NABE), Ocean Weathership Station India (OWSI), and EUMELI), spanning a range of biogeochemical environments. In particular, for these locations they were able to quantify simultaneously the nitrate transports due to processes including winter convection, turbulent mixing, and mesoscale upwelling. We still lack an observational equivalent of this study.

More generally, there is a scarcity of observational estimates for the nutrient flux due to mesoscale phenomena using the necessary high-resolution coincident in situ nitrate and physical data over a representatively large area, either for direct estimates of budgets or for validating models. While there are some estimates for the flux associated with isolated features such as eddies [e.g., *McGillicuddy et al*., 2007] or well-defined fronts [e.g., *Naveira-Garabato et al*., 2002; *Allen et al*., 2005], for an accurate picture of the role of the mesoscale we need to know the size of the contribution in a "typical" area (here taken as a square) of ocean. We are now aware that we can expect to find a dynamic and varied assortment of interacting eddies and fronts in any region a hundred kilometers or more across. What we do not have, however, is an estimate of the nitrate transport due to the joint contributions and interactions of such features in this complex but standard situation.

To illustrate the problems facing us, the current study seeks to quantify the role of mesoscale vertical nitrate fluxes to the euphotic zone for a typical region of open ocean. We do this by using measurements from a high-resolution spatial survey in the vicinity of the historic Ocean Weathership Station India (59°N, 19°W) in the Iceland Basin. The survey area contained considerable mesoscale activity, notably including a dipole comprising an asymmetrical pairing of cyclonic and mode water eddies separated by a strong jet [*Pidcock et al*., 2013]. The presence of multiple, dynamic features in the survey region makes this a good example with which to examine the difficulties currently precluding an accurate estimate of the mesoscale nitrate transport for a generic square of ocean and consequently imposing a major uncertainty on our nitrogen budgets. Note that because of the resolution of the survey we can only with confidence consider the mesoscale here, as we will only partially resolve processes at the submesoscale (1–10 km) at best. However, the issues highlighted apply also to the submesoscale. Also, attention is here restricted to vertical fluxes associated with internal ocean dynamics, and we do not, for example, consider the field of circulations involving wind forcing [e.g., *McGillicuddy et al*., 2007; *D'Asaro et al*., 2011; *Rumyantseva et al*., 2015]. For clarity, throughout we refer to the movement of nitrate at a point as the flux and the areal mean of the flux across an area of interest as the transport.

Section 2 of this paper summarizes the survey approach, instrumentation, data collection, and the diagnosis of local nitrate fluxes from coincident vertical velocity and in situ nitrate data. Section 3 presents the results in terms of the diagnosed spatial variability in local nitrate flux and the net transport for the survey region at specific depth levels. The implications of these results for estimating mesoscale nitrate supply in situ are discussed in section 4, including the contribution of mesoscale nitrate flux relative to other physical processes. Final conclusions are presented in section 5.

2. Methods

2.1. Survey Design

Data were collected as part of a research cruise to the Iceland Basin (Figure 1a) carried out between 24 July and 23 August 2007 [*Allen*, 2008]. Daily, near-real-time satellite altimetry and ocean color images for the northeast North Atlantic were used early in (and prior to) the cruise period, alongside current vector data from the vessel mounted Acoustic Doppler Current Profilers (VM-ADCPs) to select an area with mesoscale activity. Mesoscale features in the selected area included an anticyclone (later diagnosed as a mode water eddy) and a cyclone, together propagating as a dipole [*Pidcock et al*., 2013]. A high-resolution in situ spatial survey was carried out by using a towed SeaSoar vehicle within a 130 km × 130 km. For context, sea surface height at the start of the spatial survey is shown in Figure 1b, indicating the widespread mesoscale variability in the area. The survey square was centered on 59° 27'N, 19° 53'W and consisted of nine closely spaced parallel tracks, approximately 14 km apart and orientated in an east-west direction. SeaSoar was successfully towed along a total of 4.5 of the survey lines, but had to be suspended on the other survey lines due to adverse weather and/or mechanical issues. During the suspension of SeaSoar activity, lowered conductivity-temperature-depth (CTD) casts were carried out along the survey lines with ~25 km along-track spacing. The total survey time for this survey (hereafter referred to as S1) was 5.3 days.

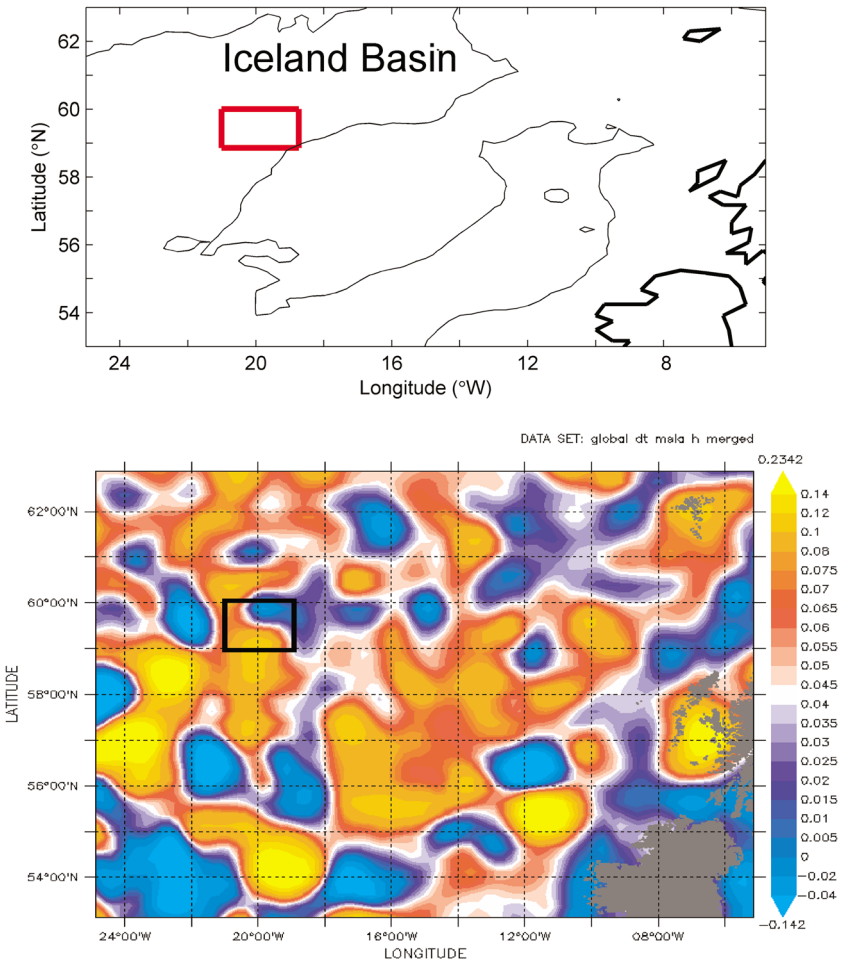

Figure 1. Location and context of survey area: (top) Map of northeast Atlantic Ocean and Iceland Basin showing location of survey area (red box centered on 60°N, 20°W) with coast (thick black line) and 1000 m bathymmetry contour (thin black line). (bottom) Satellite image of sea level anomaly for the same area showing mesoscale activity at the start of the spatial survey. Note the arbitrary scale.

A second SeaSoar survey was also carried out (hereafter referred to as S2) as a transect to bisect each eddy core and the central jet of the dipole (track marked on Figure 3c). This survey could not be used in the diagnosis of vertical velocity or, subsequently, of nitrate transport because it did not adequately map the horizontal variability of the area. However, this targeted "dogleg" section through both eddy cores is useful for characterizing the vertical nitrate distribution across the dipole (section 3.3).

The SeaSoar carried a Chelsea Technologies Group Minipack for conductivity, temperature, and pressure; a Seabird SBE43 dissolved oxygen sensor; a Chelsea TG Hemispherical Photosynthetically Active Radiation (PAR) sensor; and a National Oceanography Centre/Valeport SUV-6 ultraviolet nitrate sensor (see section 2.2). Average ship speed during SeaSoar deployments was 4.4 m/s, corresponding to an average SeaSoar vertical descent/ascent rate of ~1.3 m s^{-1} and a vertical data resolution of 1.3 m. This tow speed and surface to 450 db profiling gave a horizontal data resolution of ~3.5 km at the surface and ~2 km at middepth.

The lowered CTD frame carried a Seabird 9/11plus CTD. A total of 19 CTD casts were carried out as part of S1, to a maximum of 800 db. Water samples were taken from all CTD casts at 5, 10, 20, 27, 32, 47, 75, 125, 200, 400, 600, and 800 dbar.

A full description of the calibration of in situ temperature and salinity data obtained from SeaSoar against independent, coincident data sets (continuous underway surface thermosalinograph, continuous CTD temperature, and conductivity sensor data and discrete bottle samples) is given in *Pidcock* [2011].

Horizontal water velocities were measured continuously throughout the survey period using a 75 kHz VM-ADCP, configured to sample over 60 bins of 16 m depth (to 960 m) and averaged over 5 min intervals.

2.2. SUV-6 Nitrate Concentration Observations

The SeaSoar vehicle carried the SUV-6 UV nitrate sensor, developed at the National Oceanography Centre in association with Valeport Ltd., Totnes (UK). The SUV-6 achieves an accuracy of ±0.2 μM for a single measurement, with a response time of 1 s [*Finch et al*., 1998]. Technical and operational details of the SUV-6 instrument are outlined in *Pidcock et al*. [2010] and *Pidcock* [2011]. For more detailed description of the components, including choice of materials, refer to *Finch et al*. [1998].

Throughout the survey, additional nitrate measurements were determined from discrete water samples taken from bottles fired during each CTD profile, at the depth levels specified in section 2.1. These were used together with discrete underway samples taken hourly (from 5 m depth) during SeaSoar deployments to calibrate the SUV-6 nitrate sensor [*Pidcock*, 2011]. Nitrate concentrations from discrete samples collected from CTD casts were also combined with the SUV-6 data to map nitrate variability across the survey region.

For consistency with standard chemical oceanography usage, nitrate and oxygen concentrations are reported in units of μM throughout. The exception to this is where they are being used to calculate fluxes and units of mmol N m^{-3} are used for consistency with the resultant flux. Note that the choice of reporting in μM or mmol N m^{-3} has no impact on the numerical value as they are equivalent.

2.3. Gridding of Data

All in situ Seasoar and CTD data (temperature, salinity, and nitrate) collected between the designated starting and ending positions for S1 were amalgamated into a single data set. The vertical profiles from both data sources were combined and gridded with 8 dbar vertical spacing to 448 dbar, resulting in 56 depth levels. For each depth level, data were mapped onto a regular horizontal 2-D grid using a Gaussian filtering routine based on the principle of Inverse Distance Weighting to facilitate calculation of horizontal gradients [*Allen and Smeed*, 1996; *Pidcock*, 2011]. The interpolated value assigned to a grid point was calculated as the weighted sum of the values of all data points that fall within a user-defined search area. For the current analysis, a length scale of 25 km was used in both horizontal directions.

2.4. Diagnosis of Vertical Velocity

The vertical velocity field in the vicinity of the dipole was derived by solving the full Quasi-Geostrophic Omega equation [*Hoskins et al*., 1978] at each point in a 3-D grid encompassing the survey area (130 km × 130 km × 450 m), following the method of *Allen and Smeed* [1996] and *Pollard and Regier* [1992]. Further details of the vertical velocity diagnosis, including the derivation of geostrophic velocity field and a full discussion of potential sources of error associated with assessing vertical velocity from in situ data, can be found in *Pidcock et al*. [2013].

2.5. Diagnosis of Nitrate Transport

The starting point for quantifying the movement of nitrate in the ocean is the equation for the time evolution of a nutrient, N, defined by equation (1),

$$\partial N/\partial t = -\underline{u}.\nabla N + \partial/\partial x(k_h \partial N/\partial x) + \partial/\partial y(k_h \partial N/\partial y) + \partial/\partial z(k_z \partial N/\partial z) + S_k \quad (1)$$

where $\underline{u}$ is the velocity vector (u, v, w), k_h is the horizontal effective difusivity, k_z is the vertical effective diffusivity, and ∇ is the vector gradient operator, with components $(\partial/\partial x, \partial/\partial y, \partial/\partial z)$. In the advection term, $\underline{u}.\nabla N$, the velocity field $\underline{u}$ can be separated into components, $\underline{u_g}$ and $\underline{u_a}$, which represent geostrophic $(u_g, v_g, 0)$ and ageostrophic (u_a, v_a, w) flows, respectively. The current study focuses on the advection of nitrate due to the vertical component of ageostrophic flow (w). Note that there is an implicit separation of scales in equation (1). The velocity $\underline{u}$ is taken to represent water movement only for scales above ~100 m. This is done on the assumption that this is roughly the scale at which the ocean circulation goes from being two-dimensional at larger scales to three-dimensional at smaller ones. The effect of the turbulent motion at smaller scales is represented as an effectively diffusive process (the second, third, and fourth terms on the right-hand side in equation (1)). This study focuses on the vertical supply of nutrients and so horizontal transport is not discussed. The fourth term on the right-hand side of equation (1), which represents the vertical transport of nutrient due to small-scale mixing, was simultaneously estimated by *Forryan et al*. [2012], allowing us to compare the magnitude of this flux with that due to vertical advection discussed in section 4. The fifth term on the right-hand side of equation (1) (S_k) represents other

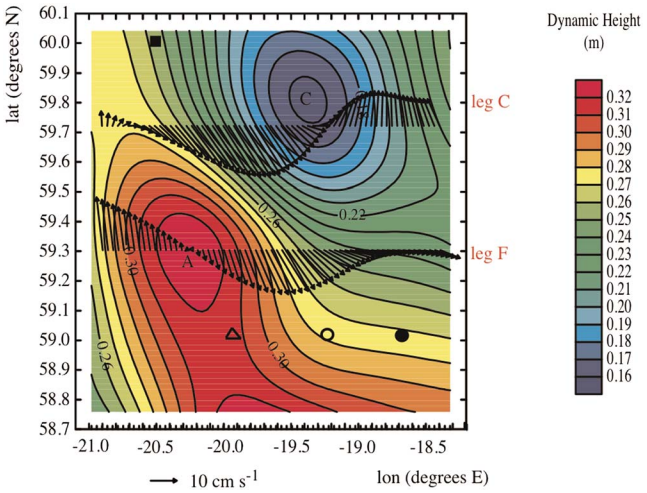

Figure 2. Contours of dynamic height at 50 m, with geostrophic velocity vectors also at 50 m for leg C (59.72°N) and leg F (59.30°N) of the spatial survey (S1). The centers of the cyclonic (C) and anticyclonic (A) eddies, according to the minimum and maximum in dynamic height, are indicated. The black symbols indicate the four CTD casts chosen to represent noneddy conditions, referred to in section 3.3.

potential sources (such as remineralization and atmospheric input) and sinks (such as biological uptake) of a nutrient.

The vertical flux of nitrate at a point is simply wN. Both w and N can be split into two components; the areal mean for the survey area at a given depth level, denoted by angle brackets ($<w>$ and $<N>$, noting that both will vary with depth), and the perturbation at a given location relative to the areal mean, denoted by w' and N', respectively, such that $w = <w> + w'$ and $N = <N> + N'$. The vertical flux at a given point can then be written as

$$wN = < w >< N > + w^{'} < N > \quad (2)$$

$$+ < w > N^{'} + w^{'}N^{'}$$

The areal mean of equation (2) over the survey area represents the net transport at a given depth. In calculating the average, the second and third terms on the right-hand side of equation (2) cancel as, by definition, the areal means of both w' and N' are equal to zero. The transport is therefore given by

$$< wN >=< w >< N > + < w^{'}N^{'} > \quad (3)$$

Note that positive movement is defined as directed upward and negative movement is directed downward.

Taking a fluid dynamical perspective, assuming that the large-scale, background flow in the surveyed region is geostrophic i.e., balanced, horizontal flow, it follows that any vertical velocity within the survey region can, in principle, be attributed to mesoscale or submesoscale perturbations to this geostrophy. This is how we define the mesoscale vertical circulation for the purposes of this paper; we assume that the scale of sampling and smoothing means that we do not capture the submesoscale (1–10 km) contribution. (The Omega equation that is used here to diagnose w does not estimate vertical motion arising from waves, tides, or inertial motions). From this perspective, the mesoscale transport can be estimated directly as $<wN>$. To illustrate the potential bias of not having a zero net vertical velocity in the survey region we also estimate $<w'N'>$, where both w' and N' are calculated relative to the mean respective values for a given survey, at a given depth [*McGillicuddy et al.*, 2003; *Naveira-Garabato et al.*, 2002]. This is analogous to the "eddy flux" often used in modeling studies. In a strict sense, this should involve averaging over a time scale chosen to match the spatial scale, ideally at a clearly defined scale separation, but here we only have one "snapshot" of the field. Nevertheless, this approach allows us to gauge the impact of the net vertical flow. If the vertical transport of water is such that $<w>$ is equal to zero, then using the total flux $<wN>$ (henceforth Method A) will give the same estimate as using the perturbation flux $<w'N'>$ (henceforth Method B). The discussion in section 4 will explore the ramifications when $<w>$ does not equal to zero.

The analysis will focus on (i) the 50 m depth surface, which corresponds to the base of the euphotic zone in the current study (estimated using the SeaSoar PAR sensor), and (ii) the 98 m depth surface (closest grid level to 100 m), in order to allow comparison with literature estimates of mesoscale nitrate flux.

3. Results

3.1. Physical Context

Figure 2 shows the dynamic height field at 50 m depth. This is overlaid with geostrophic velocity vectors (also at 50 m) for S1 survey legs C and F (see Figure 3a for full S1 track), which passed close to the centers of the cyclonic and anticyclonic eddies, respectively. The cyclonic (anticyclonic) component of the dipole is clearly

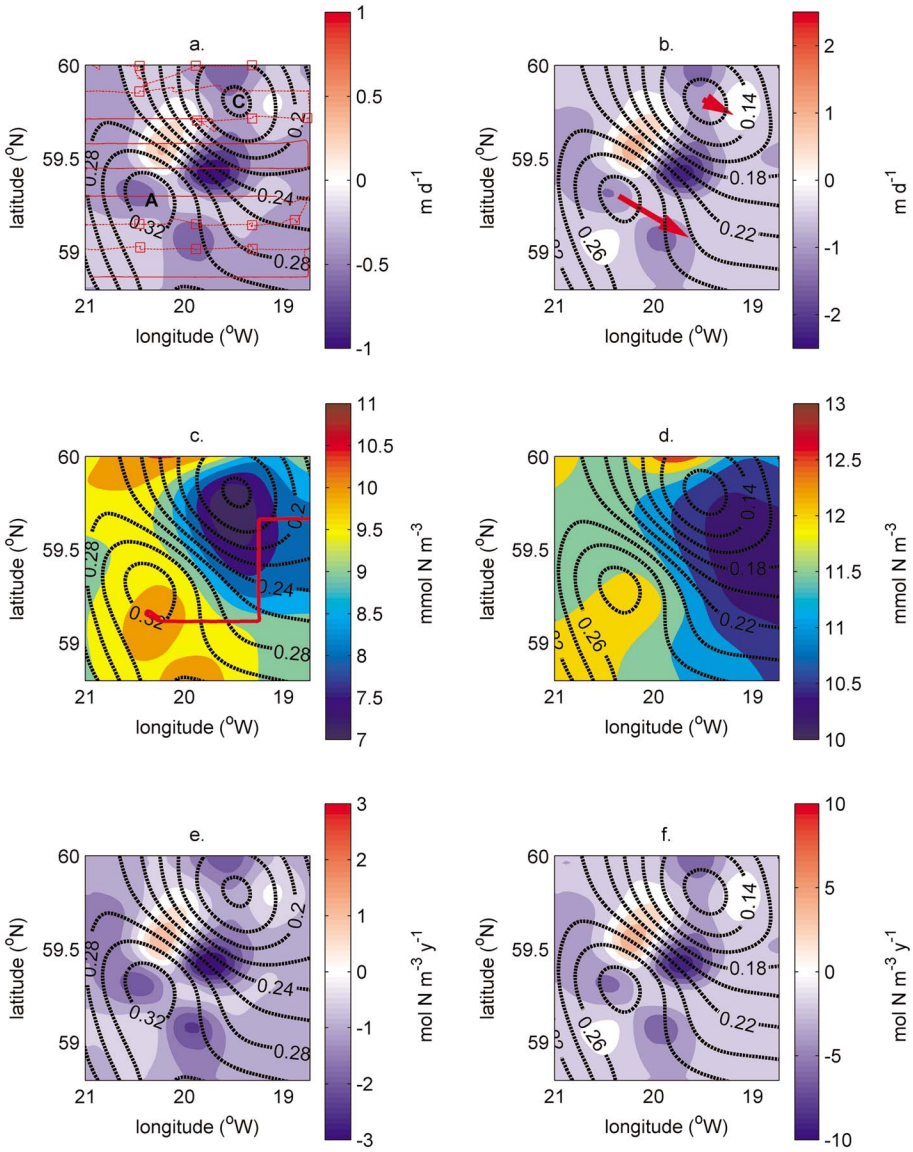

Figure 3. (a and b) Vertical velocity (m d^{-1}) at 50 m and 98 m, respectively. Upward is positive. The centers of the cyclonic (C) and anticyclonic mode-water (A) eddies are indicated in Figure 3a. The solid red line and red boxes in Figure 3a represent where in situ physical data date were collected using SeaSoar and lowered CTD, respectively. The dashed red line represents the ship's track and indicates where ADCP data exist but SeaSoar data do not. The red arrows in Figure 3b show the direction of propagation of the two eddies. (c and d) Nitrate concentration at 50 m and 98 m, respectively. The red line in Figure 3c indicates the track taken on the dog-leg transect shown in Figure 4. (e and f) Nitrate flux at 50 m and 98 m, respectively. Upward is positive. The black lines in all panels indicate dynamic height contours at 50 m and 98 m, respectively, with 1 cm intervals.

reflected in a lower (higher) dynamic height of −0.08 m (+0.07 m) relative to the central jet between the eddies. An analysis of deep CTD casts within the vicinity of the anticyclonic eddy revealed this component of the dipole to be a mode water eddy, with a deep homogenous core centered at 600 m (~8.8°C and ~35.28 practical salinity unit), extending down to over 1000 m [*Pidcock et al.*, 2013]. Peak in situ and geostrophic velocities of ~60 cm s^{-1} and ~22 cm s^{-1}, respectively, were found in the southeastward flowing central jet between the counterrotating eddies at approximately 300 m.

3.2. Vertical Velocity

The full analysis of the vertical velocity field resulting from the mesoscale dynamics in this region is described by *Pidcock et al.* [2013], where the three-dimensional vertical velocity field is reconstructed. However, it is

Table 1. Means (<>), Standard Deviations (σ), Correlations, and Transports at 50 m and 98 m

	50 m	98 m	
$<N>$ (mmol m^{-3})	9.13	11.28	
$<w>$ (m d^{-1})	−0.23	−0.38	
$\sigma(N)$ (mmol m^{-3})	1.88	1.00	
$\sigma(w)$ (m d^{-1})	0.24	0.59	
Spearman correlation	0.29	0.14	
$<wN>$ (mol N m^{-2} yr^{-1})	−0.76	−1.54	Method A
$<wN>$ (mmol N m^{-2} d^{-1})	−2.08	−4.2	
$<w'N'>$ (mol N m^{-2} yr^{-1})	+0.0082	+0.0069	Method B
$<w'N'>$ (mmol N m^{-2} d^{-1})	+0.022	+0.019	

useful to review briefly the main characteristics of the vertical velocity distribution here (Figures 3a and 3b) ahead of the diagnosis of local and net nitrate transport.

The main activity in terms of vertical motion occurs in the central jet where a strong upward vertical velocity (up to 3.6 m d^{-1} at 450 m —not shown—but ~1 m d^{-1} at 98 m; Figure 3b) is found directly upstream (centered on 59.6°N, 20.2°W) of stronger downward vertical velocity (up to 5.0 m d^{-1} at 450 m—not shown—but ~2 m d^{-1} at 98 m; Figure 3b). This spatial pattern is due to fast-flowing water in the jet moving over an upward deflection of isopycnals associated with the cores of the flanking eddies overlapping vertically. Near-zero or relatively weak vertical velocities (centered on 59.8°N, 19.1°W and 59.0°N, 20.5°W, respectively) existed ahead of the cyclonic (+0.5 m d^{-1} at 450 m but ~0 at 98 m) and mode water (−2.5 m d^{-1} at 450 m but ~ −1 m d^{-1} at 98 m) eddies in the direction of propagation. The boundary of the mode water eddy was found to inhibit lateral transport, resulting in a diminished contribution to total vertical velocity from transport along isopycnals raised above the mode water core. The spatial variability in the vertical velocity field at 50 m and 98 m (shown in Figures 3a and 3b, respectively) has a strong influence on the distribution and transport of nitrate across the dipole (section 3.4). As may be apparent to the eye, a negative <w>, i.e., average vertical velocity downward, is found for the sampling region at both 50 m and 98 m (see also Table 1). This is contributed to by the greater

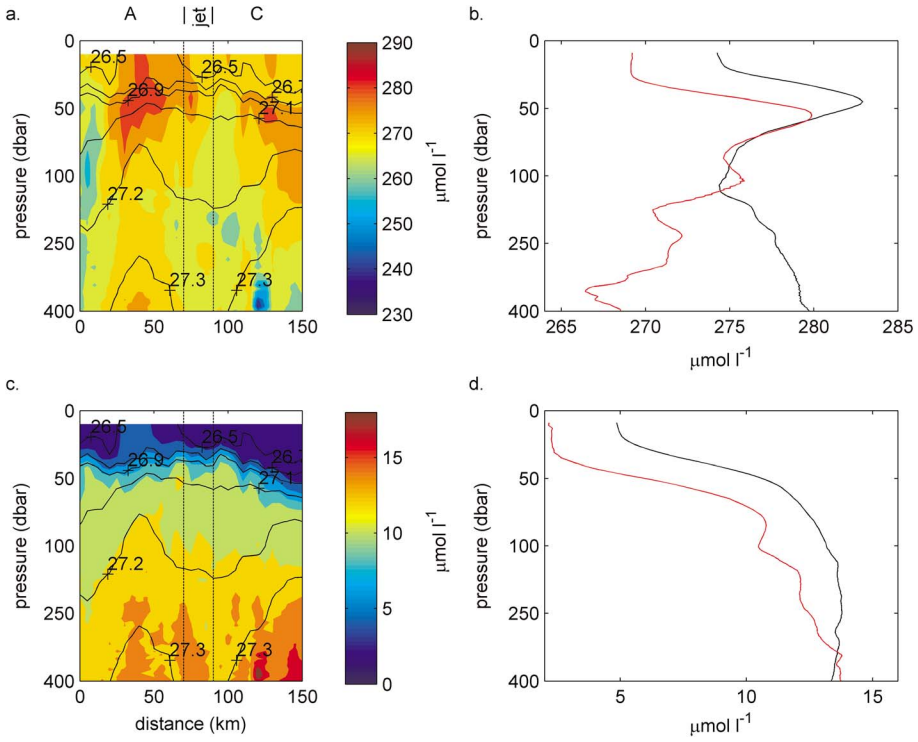

Figure 4. Vertical section through the dipole showing (a) dissolved oxygen concentration (μM) and (b) nitrate concentration (μM) over the full depth range of SeaSoar (0–450 m) for the dogleg section marked in Figure 3c. The *x* axis represents distance in kilometers from the beginning of the section. The black solid lines indicate isopycnals of potential density (kg m^{-3}). The anticyclonic (A), cyclonic (C), and jet components of the dipole are identified based on isopycnal displacement and are indicated by the vertical dashed lines. Mean (b) oxygen (μM) and (d) nitrate (μM) vertical profiles for the anticyclone (black) and cyclone (red). For all panels note the exploded scale above 100 m to better show surface structure.

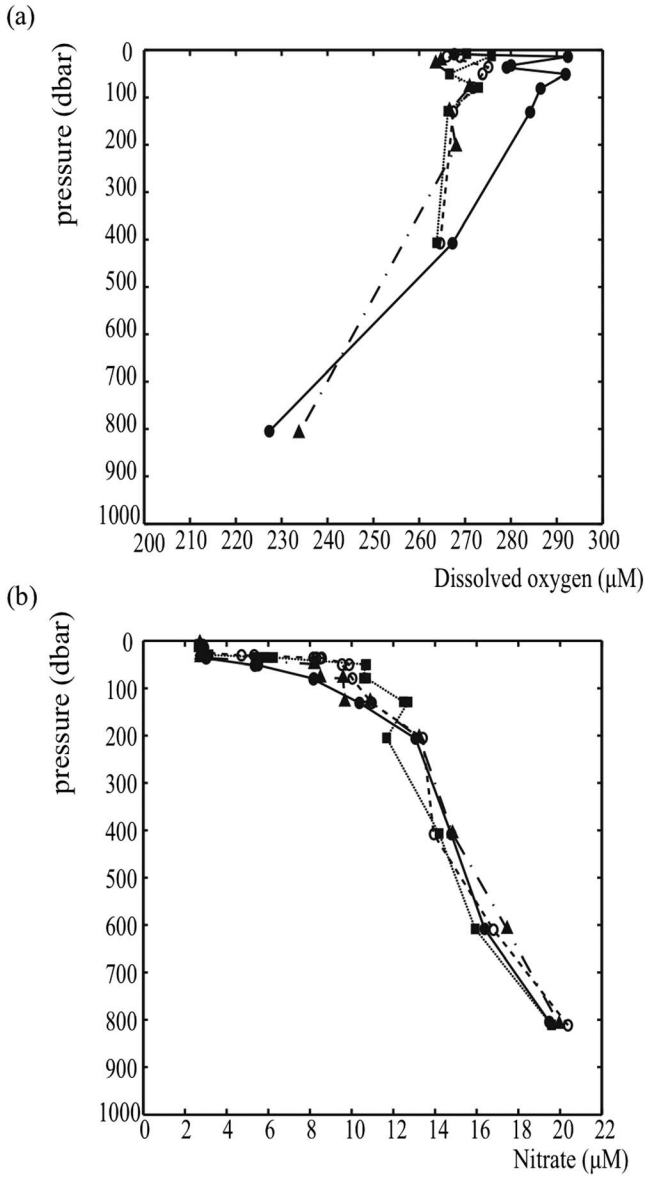

Figure 5. Vertical profiles of (a) dissolved oxygen concentration (μ*M*) and (b) nitrate concentration (μ*M*) from bottle samples collected from deep (0–1000 m) CTD casts deemed to be in "noneddy" locations (positions indicated in Figure 2). The same four casts are shown in Figures 5a and 5b although oxygen samples were taken below 400 m in only two of the four casts. The symbols match those denoting the positions of samples in Figure 2.

magnitude of localized downward vertical velocity in the identified dynamical features (particularly in the central jet) than upward vertical velocity, plus the existence of a weak negative vertical velocity over the majority of the survey area outside these localized "hot spots" [see also *Pidcock et al*., 2013].

3.3. Nitrate Distributions

Isopleths of nitrate below 100 m shoaled toward the center of both eddies, largely coincident with the doming of isopycnal surfaces (Figure 4c). Surface nitrate concentrations were higher above the mode water eddy than the cyclonic eddy (~5 μ*M* compared to ~2 μ*M*, respectively; Figure 4c), likely due to the greater shallowing of isopycnals from the thermocline. However, surface concentrations were not low enough to limit phytoplankton growth anywhere in the surveyed region. Availability of iron is thought to be the limiting factor in the Iceland Basin postbloom [*Nielsdóttir et al*., 2009].

There is a clear impression of the dipole at 50 m (Figure 3c), where the mode water and cyclonic eddy centers are associated with nitrate concentrations of ~10.4 μ*M* and 6.8 μ*M*, respectively. At 98 m, the pattern is less clear (Figure 3d) although, broadly speaking, the mode water eddy is associated with higher nitrate concentrations than the cyclonic eddy. A tongue of high nitrate (9.5 μ*M*) water extends from close to the mode water core in a southwestward direction at 50 m. This tongue is narrower and restricted to the southwest at 98 m. The consistent differences in nitrate concentration between the eddies with depth can be seen in the vertical profiles shown in Figure 4d. There are high nitrate concentrations on the northern boundary of the survey area at 98 m (reaching 12.8 μ*M*), plus a further small region in the north west corner toward the Reykjanes Ridge, but lying at the edge of the survey area the data are too limited to draw any conclusions about upstream effects. The central jet itself exhibits an intermediate nitrate concentration of ~11.5 μ*M* at 98 m. A large area in the eastern part of the survey region, which extends to the south of the cyclonic eddy, contains relatively low nitrate concentration (~10.5 μ*M*) water at 98 m.

Although nitrate concentration is clearly influenced by the eddy-scale density distribution, considerable spatial variability can be observed in Figure 4c at scales down to 5 km. The maximum nitrate concentration in Figure 4c (20 μ*M*) is found in a very localized area toward the periphery of the cyclonic eddy, approximately

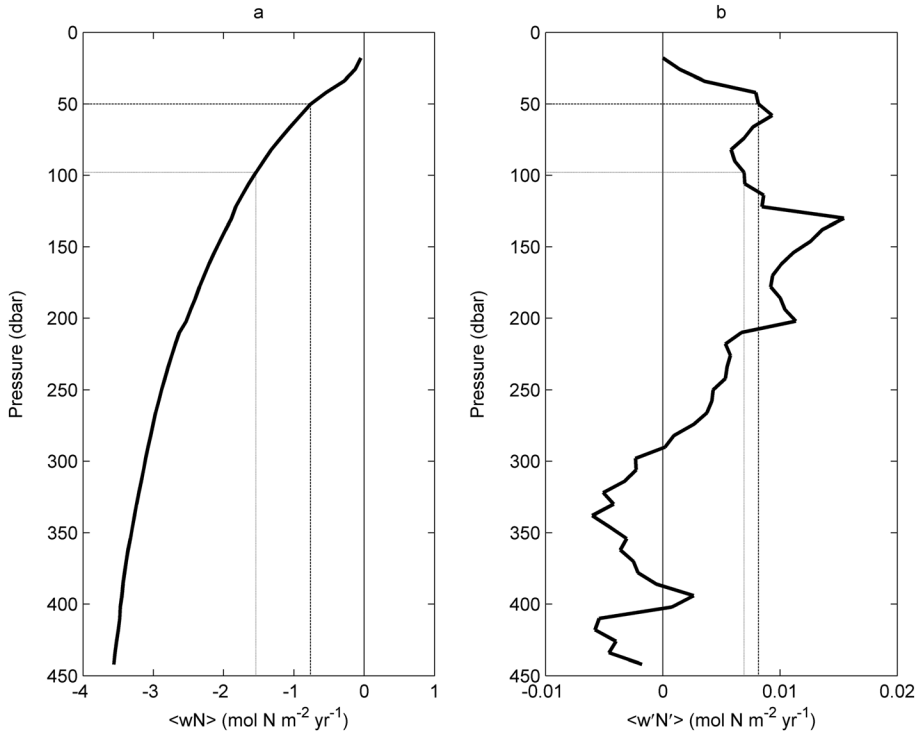

Figure 6. Vertical profiles of areal mean nitrate transport. Vertical profiles of (a) $<wN>$ (mol N m^{-2} yr^{-1}) and (b) $<w'N'>$ (mol N m^{-2} yr^{-1}) over the full depth of SeaSoar (0–450 m). Zero on the transport is indicated by the dark grey solid line. Transport at 50 m and 98 m is also indicated in each image.

120 km from the start of the section and at a depth of ~375 m. A comparison with the four CTD casts furthest from the influence of the eddies as possible (positions marked on Figure 2b) shows that the joint oxygen and nitrogen signatures of 238 μM and 20 μM, respectively (Figures 4a and 4c), are consistent with water found at ~800 m (Figure 5) elsewhere in the region, indicating very localized upward transport of water of over 400 m to its present location. Although the implications of such submesoscale features on the vertical injection of nutrients within the region cannot be quantified in the present study, the role of the submesoscale is discussed further in section 4.

3.4. Local Nitrate Flux and Areal Net Transport

3.4.1. Method A (*wN*)

The spatial distribution of the nitrate flux *wN* at 50 m and 98 m is shown in Figures 3e and 3f, respectively. The absolute value of *N* (from which *wN* is calculated) can only be positive in sign. Therefore, the distribution of upward and downward flux is set by the spatial pattern of the absolute velocity field (Figures 3a and 3b); regions of upward vertical velocity are associated with positive nitrate flux and vice versa. There is an important difference in the spatial distribution of vertical velocity and nitrate. Specifically, while the distribution of *w* reflects the localized nature of the vertical velocity features discussed in section 3.2, variability in the nitrate data is generally at larger scales. The nature of the correlation of nitrate and vertical velocity is explored more quantitatively in section 4.

Fluxes reach a maximum of ~6 mol N m^{-2} yr^{-1} at 98 m. Note that to make the conversion of in situ nitrate concentration to units of transport clearer, nitrate concentration is expressed in terms of mmol m^{-3} (which are equivalent to μM to reasonable accuracy) here and onward.

The vertical profile of the areal mean transport $<wN>$ at each depth level in the 3-D grid is shown in Figure 6 a. A negative net transport of magnitude increasing with depth is observed, from close to zero at the surface to ~ −3.5 mol N m^{-2} yr^{-1} at 450 m. The value of $<wN>$ at 50 m is −0.76 mol Nm^{-2} yr^{-1}. At 98 m, the transport is −1.54 mol N m^{-2} yr^{-1} (Table 1).

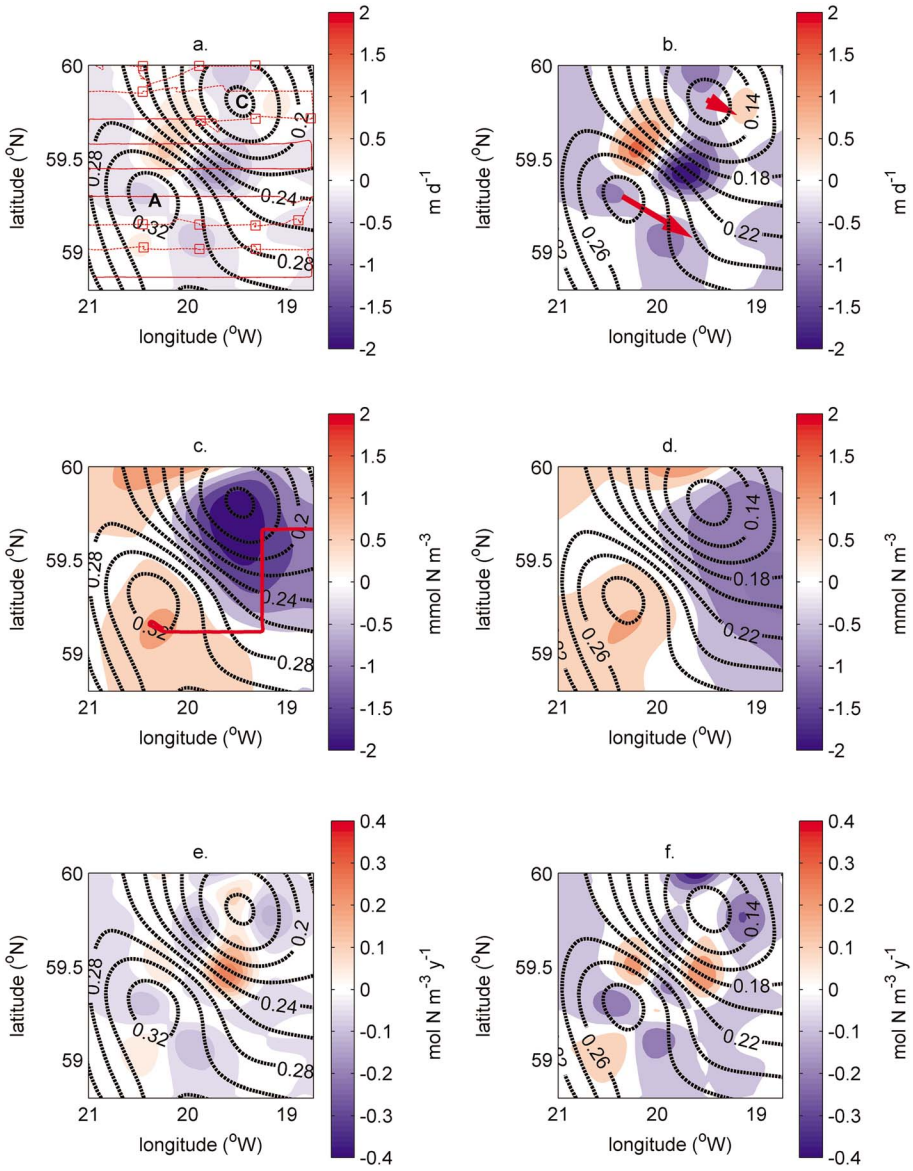

Figure 7. As Figure 3 but showing anomalies. (a and b) Vertical velocity anomaly, w' (m d^{-1}), at 50 m and 98 m, respectively. (c and d) Nitrate concentration anomaly, N' (mmol N m^{-3}), at 50 m and 98 m, respectively. (e and f) Nitrate flux anomaly, $w'N'$ (mmol N m^{-2} d^{-1}), at 50 m and 98 m, respectively.

3.4.2. Method B ($w'N'$)

The spatial distributions of N' and w' at 50 m and 98 m are shown in Figure 7. They are calculated by using values of $<N>$ and $<w>$ at each depth, respectively (Table 1). The spatial pattern of anomalies for vertical velocity, w' (Figures 7a and 7b), and nitrate concentration, N' (Figures 7c and 7d), is the same as those for w and N. However, because the nitrate anomaly, N', can be positive or negative, the spatial pattern of positive and negative fluxes, $w'N'$, is no longer set solely by the corresponding pattern for vertical velocities. A consequence of this is that the dipole pattern of strong upward flux in the northwest of the jet with strong downward flux downstream in the southeast of the jet for wN becomes a quadrupole pattern for $w'N'$ due to the nitrate anomaly changing sign either side of the jet. Furthermore, there are regions where a positive flux exists by virtue of negative values of w' being associated with a negative nitrate anomaly (i.e., not by the upward transport of relatively nitraterich water but by the downward transport of relatively nitrate poor water). An example of this can be found downstream on the northeastern side of the central jet.

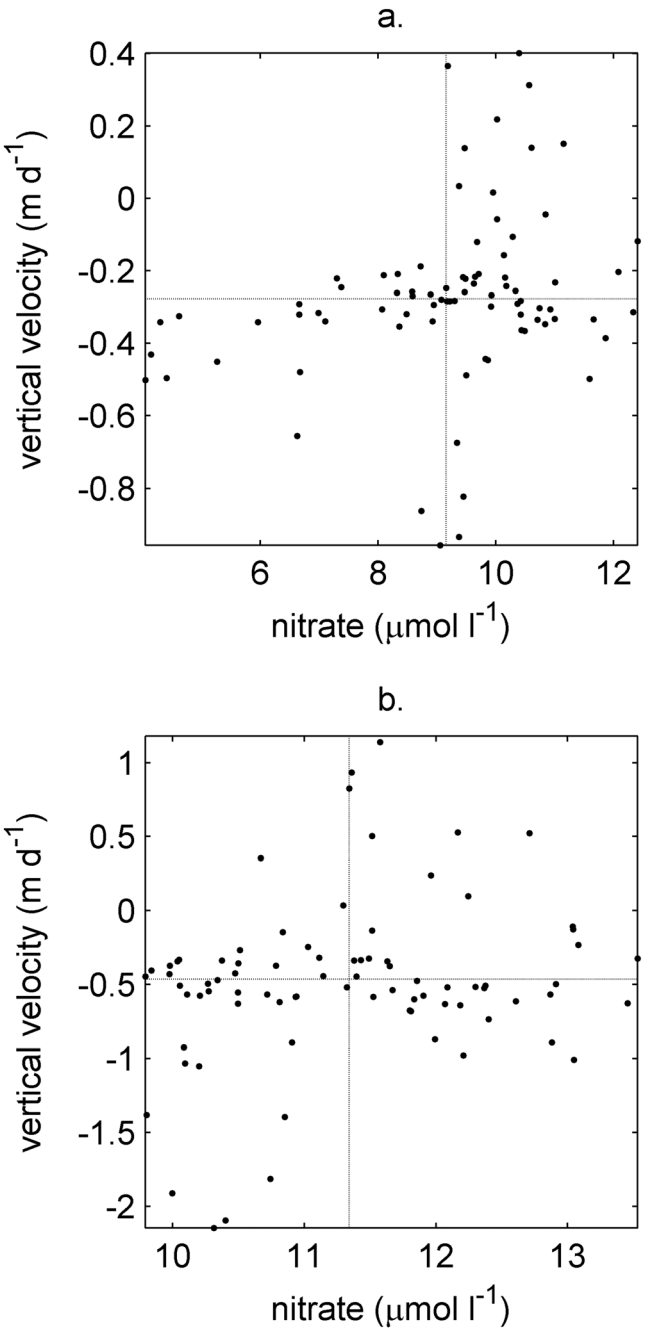

Figure 8. Scatterplot of vertical velocity (w) (m d^{-1}) against nitrate concentration (N) (μmol l^{-1}) for all data points at (a) 50 m and (b) 98 m. The lines show mean for w and N.

Another example of the influence of negative nitrate anomalies can be found ahead of the propagating eddies. The weakly upward vertical velocity ahead of the cyclonic eddy in the direction of propagation and the downward vertical velocity ahead of the mode water eddy are both associated with negative nitrate transport, at both depths and of similar magnitudes of 0.2 mol N m^{-2} yr^{-1}, due to having negative and positive nitrate anomalies associated with them, respectively.

Local nitrate fluxes are an order of magnitude larger using Method A than Method B because of the large mean nitrate concentration relative to the magnitude of anomalies at each depth.

The vertical profile of areal mean transport $<w'N'>$ for each depth level of the 3-D grid is shown in Figure 6b. A net upward transport of nitrate exists above ~250 m, and a net downward transport is found below ~250 m such

Table 2. Literature Comparison of Areal Mean Mesoscale Nitrate Transport[a]

	$\langle w'N' \rangle$	$w_{RMS}\langle N \rangle$	$\langle wN \rangle$
Naveira-Garabato et al. [2002]	−0.04[b]	-	-
Lapeyre and Klein [2006]	-	+0.08–0.26[b]	-
Present study	+0.0069[c]	+1.16 [b]	−1.54[b]

[a]All figures in (mol N m^{-2} yr^{-1}).
[b]Net flux at 100 m.
[c]Net flux at 98 m.

that, by using Method B the net transports across the survey area at the base of the euphotic zone (50 m) and at 98 m are calculated to be +0.0082 mol N m^{-2} yr^{-1} and +0.0069 mol N m^{-2} yr^{-1}, respectively (Table 1). Comparing to the value of $\langle wN \rangle$ at 50 m (−0.76 mol Nm^{-2} yr^{-1}), there is a difference in the value of the transport by 2 orders of magnitude, together with a reversal in the sign from positive to negative. At 98 m, the transport differs from the value obtained in Method A (−1.54 mol N m^{-2} yr^{-1}) by a factor of over 200. As at 50 m, this increase in magnitude is also associated with a change in sign, from net positive to net negative transport.

4. Discussion

4.1. The Correlation Between Nitrate and Vertical Velocity

In the absence of simultaneous nitrate estimates to quantify the impact of mesoscale-driven processes on nitrate supply to the upper ocean it might be tempting to make the assumption that positive (upward) vertical velocities are associated with bringing up nitrate-rich water from below the thermocline and that negative (downward) vertical velocities transport water down from the nutrient-poor upper sunlit layers of the ocean. To examine whether there is such a correlation between vertical velocity and in situ nitrate concentration, in Figure 8 we present scatterplots of w against N at (a) 50 m and (b) 98 m (note that S2 is not used for this analysis as a reliable vertical velocity diagnosis is not possible as a result of the sampling pattern—see section 2.1). Applying Spearman's rank method, to allow for a nonlinear relationship, the correlation between nitrate concentration and vertical velocity is found to be weak: $r = 0.29$, $p = 0.01$ at 50 m; $r = 0.14$, $p = 0.19$ at 98 m (Table 1).

Lapeyre and Klein [2006] calculated the nitrate transport at 100 m in a numerical simulation of a turbulent eddy field. They used wavelet analysis to identify regions of the model occupied by eddies and filaments. They then used the root-mean-square w'at 100 m (1.65 m d^{-1}) for these regions, and an assumed mean nitrate concentration (N) at 100 m (1.5 μM) to estimate the vertical transport. To do this they assumed that half of the area covered, e.g., by eddies (17%) vertically advected water with $N = 1.5$ μM upward and advected the same amount of water downward with no nitrate content (i.e., assuming 100% efficiency of nitrate use by phytoplankton in the euphotic zone). The method effectively imposes a horizontal distribution of nitrate at 100 m that is correlated with the vertical velocity field; i.e., where there are upward vertical velocities, there will be high nitrate concentrations, and where there are downward vertical velocities, there will be low nitrate concentrations. This inevitably results in a positive net transport across the selected depth level. The authors report a net nitrate transport at 100 m of +0.08 mol N m^{-2} yr^{-1} if just eddies are considered or +0.26 mol N m^{-2} yr^{-1} if filaments are included (Table 2). As the model resolution was ~2 km it resolves further into the submesoscale than our study and so the value for comparison probably falls between these two values.

If a similar method is applied to calculate the transport of nitrate at 98 m in the present study, an areal mean nitrate concentration (N) at 98 m of 11 μM (Table 1) and a RMS w' over the survey area of 0.56 m d^{-1} yields a net nitrate transport at 98 m of +1.16 mol N m^{-2} yr^{-1}. This is of similar magnitude to the transport estimated using Method A (−1.54 mol N m^{-2} yr^{-1}) but of opposite sign and uses a nitrate concentration an order of magnitude larger than in *Lapeyre and Klein* [2006]. Compared to the diagnosed net transport using Method B at 98 m (+0.0069 mol N m^{-2} yr^{-1}) this represents an increase in the nitrate transport by a factor of ~150. The discrepancy occurs because in many parts of our survey area downward vertical currents transport water that is elevated in nitrate relative to the areal mean at that depth, resulting in a significantly lower net upward transport than obtained in the idealized scenario.

One approach to avoid having to make assumptions about correlations is to make use of an empirical relationship between nitrate concentration and another variable whose distribution is better known/more easily sampled. Multiyear time series data, e.g., from the Bermuda Atlantic Time Series (BATS) [*McGillicuddy and Robinson*, 1997; *Siegel et al.*, 1999] have indicated a strong nitrate-potential density correlation ($r^2 = >0.8$) in the upper part of the main thermocline (400–600 m). The assumption of a direct correlation between nitrate

Table 3. Literature Comparison of the Range of Local Nitrate Fluxes[a]

	$w'N'$	wN
Naveira-Garabato et al. [2002]	−0.35/+0.79[b]	-
Present study	−0.40/+0.30[c]	−9.2/+5.3[c]

[a]All figures in mol N m^{-2} yr^{-1}.
[b]Minimum and maximum values at 100 m.
[c]Minimum and maximum values at 98 m.

and density formed the basis for estimates of the influence of mesoscale eddies on vertical nitrate transport, known as "eddy pumping" [*Falkowski et al.*, 1991; *McGillicuddy et al.*, 1999; *McGillicuddy and Robinson*, 1997; *McGillicuddy et al.*, 1998; *Martin and Pondaven*, 2003; *Oschlies*, 2002; *Siegel et al.*, 1999]. The time series did not include vertical velocity estimates, however. Instead, the vertical displacements of isopycnals associated with isolated eddy features were used in conjunction with the nitrate-density relationship to estimate the vertical transport due to mesoscale features. Neverthless, such studies were instrumental in highlighting the potential importance of mesoscale circulations on the vertical nitrate transport.

Naveira-Garabato et al. [2002] used a similar empirical approach to calculate the net nitrate transport associated with a meander of the Antarctic Polar Front (APF) and attendant cyclonic and anticyclonic circulations. They collected local in situ nitrate data during a series of full-depth CTD casts over two meridional transects (out of 13 parallel SeaSoar survey tracks) and at regular intervals from the ship's underway supply. An algorithm relating nitrate concentration to salinity at these stations was then used to infer the nitrate concentration at each point in the 3-D vertical velocity grid from the local salinity. The net vertical velocity across the survey area was zero: the survey contained a full wavelength of a meander and both a cyclonic and an anticyclonic circulation. The range in local flux of −0.35 to +0.79 mol N m^{-2} yr^{-1} at 100 m obtained by *Naveira-Garabato et al*. [2002] is of similar magnitude to that obtained in the present study at 98 m of −0.40 to +0.30 mol N m^{-2} yr^{-1} (Table 3), though their nitrate concentration at 100 m (25 μM) was more than double than ours. A net downward transport of nitrate was found at all depths, with a peak magnitude of −0.095 mol N m^{-2} yr^{-1} near 250 m. Previous estimates of the net subduction of nutrient-rich water in the region of the Antarctic Polar Front [*Nelson and Smith*, 1991] were put forward as consistent with this estimate. The net transport at 98 m (calculated using $w'N'$ to be consistent with *Naveira-Garabato et al*. [2002]) in the present study of +0.0069 mol N m^{-2} yr^{-1} is an order of magnitude smaller than that obtained by *Naveira-Garabato et al*. [2002] at 100 m (−0.04 mol N m^{-2} yr^{-1}), and in the opposite direction (Table 2). Part of the discrepancy stems from the different concentrations of nitrate at 100 m. This still leaves a difference that is fivefold in magnitude and opposite in sign to reconcile. The horizontal pattern of vertical velocities used in the *Naveira-Garabato et al*. [2002] estimate can be seen in Figure 6 of *Naveira-Garabato et al*. [2001]. It shows velocities at 189 m rather than 100 m, but the pattern should be very similar. Comparing this to the horizontal pattern of nitrate distribution shown in Figure 5a of *Naveira-Garabato et al*. [2002], it is seen that there is a large-scale gradient in nitrate concentration from northwest to southeast, mimicking the density field, but vertical velocities concentrated at smaller scales. This difference in scales is similar to our study. However, in the case of *Naveira-Garabato et al*. [2002] the region of negative N' (the northwestern part of the domain) contains predominantly positive velocities, whereas the region of positive N' (the southeast) is roughly balanced in positive and negative transports. The northwestern area therefore drives the negative net downward transport for the region. In our study, the distribution of upward and downward velocities gives a closer balance in nitrate transport. It is curious but possibly a coincidence that the "simpler" setting of a meandering front gives a larger transport than a more complicated flow involving several eddies and a jet. Nevertheless, the consistent contrast in scales between w' and N' does suggest an interesting hypothesis for future work to test: that nitrate variability largely echoes mesoscale variability in density, but strong vertical velocities are focused at smaller scales, often at boundaries of mesoscale features, such that the correlations between w' and N' are inevitably weak, leading to small average nitrate transport despite strong localized upwelling. Further work should also consider the role of biological uptake in influencing this transport via its effect on nitrate gradients.

4.2. How Accurately Can We Estimate the Mesoscale Nitrate Transport for the Area?

The accuracy of our estimate for the nitrate flux at a given location is dependent on the accuracy of our determinations of w and N. Uncertainty in N arises from the sensitivity of the SUV-6 nitrate sensor, found to be 0.2 mmol N m^{-3} by *Pidcock et al*. [2010]. For w, an analysis by *Pidcock et al*. [2013] quantified errors due to spatial resolution of sampling (50%), lack of synopticity (20%), and the length-scale chosen to grid data (25%),

giving an estimated uncertainty of ~95%. While the combined effect of these uncertainties can change estimates for transport by a factor of 2, a potentially more important issue is highlighted by the 2 order of magnitude and sign difference between estimates using Methods A and B.

The discrepancy arises from the contribution of the mean fields. Away from the surface where nutrients may be exhausted, the mean nitrate concentration at a depth rapidly becomes dominant in magnitude compared to anomalies (Table 1). The impact that this has on the difference between Method A and B estimates, however, is controlled by the net vertical velocity for the region. If the net vertical velocity is zero then Method A and B agree regardless of the magnitude of the mean nitrate concentration. For our study the net vertical velocity is nonzero and large enough to introduce the large disparity seen (Table 1). Another survey might be fortunate in choosing a square where the effects of all the eddies and fronts within it are balanced giving $<w>=0$, but given the dynamic nature of mesoscale features this is unlikely to be true for the same square just a few days later, let alone in another randomly chosen square. Given the strong influence of the mean fields, to have an accurate estimate of the typical mesoscale nitrate flux we need to know the expected net vertical velocity at the mesoscale for a typical square of open ocean. Without this information we do not know how biased are individual estimates, such as the one presented here.

Time series may provide a better means of tackling this. Using mooring data *Sévellec et al.* [2015] demonstrated that the time mean of vertical motion due to mesoscale processes is indistinguishable from zero integrated over a year. However, the vertical circulation varied considerably in time and on any day within that year could be significant. An obstacle to applying such an averaging approach to estimating the mesoscale nitrate transport spatially is that it would require a substantially larger survey area to encompass an equivalent number of mesoscale features. This poses a problem for synopticity. The survey reported here took 5.3 days, already near the limit if one wants to avoid the circulation that is being mapped changing significantly in the interim [e.g., *Allen et al.*, 2001]. Lack of synopticity can also lead to offsets in positions of estimated vertical velocities relative to real ones [*Allen et al.*, 2001], which may reduce a correlation with nitrate should one be present. (The patterns of nitrate and vertical velocity in this study, however, are sufficiently different in spatial structure for this not to be an explanation of the weak correlation.)

Given the sensitivity of nitrate transport estimates to chance in the choice of the survey area and even of the days on which it is mapped, it is unclear how the typical mesoscale nitrate transport can be estimated spatially using current technology. While such studies are still vital in understanding how specific mesoscale supply mechanisms operate [e.g., *Thomas et al.*, 2013], a reliable estimate of the net mesoscale contribution to nitrate budgets may be best sought in time series.

4.3. Budgetting Nitrate Supply

We now examine the relative contribution of the mesoscale to the vertical budget of nitrate supply by comparing our estimates both to those arising from other physical processes and, first, to the uptake of nitrate by phytoplankton within surface waters as a proxy upper limit on vertical nitrate delivery.

4.3.1. Biological Uptake

Measurements of nitrate uptake by phytoplankton were carried out at a total of 13 stations during the D321 survey period (M. Lucas, unpublished data). Uptake rates integrated above 50 m during the cruise (mmol N m^{-2} d^{-1}) were converted into an integrated rate per year (mol N m^{-2} yr^{-1}) simply by multiplying by 365. Note that this change of units is purely to allow comparison to other sources of nitrate in the following sections. The figures should not be taken as an extrapolated estimate of the amount of nitrate uptake over the year; because this cruise took place in summer such integrated annual nitrate uptake rates are likely to be underestimates. Integrated NO_3 uptake across all stations ranged from 0.3 to 1.1 mol N m^{-2} yr^{-1} with a mean value of 0.66 mol N m^{-2} yr^{-1} (Lucas, personal communication). These values are lower than previous in situ estimates for the northeast Atlantic of ~2–3 mol N m^{-2} yr^{-1} in spring/summer [*Boyd et al.*, 1997; *Sambrotto et al.*, 1993] and ~3.0 mol N m^{-2} yr^{-1} in June/July [*Jickells et al.*, 2008].

The net mesoscale nitrate transport calculated from $<wN>$ in the present study at 50 m (comparable with the depth of the 1% light level) is comparable to uptake (0.76 and 0.66 mol N m^{-2} yr^{-1}, respectively). However, as already noted, the mesoscale transport is away from rather than toward the euphotic zone due to the considerable bias resulting from the existence of a negative $<w>$.

Locally, the maximum upward nitrate transport calculated from *wN* in the present study (5.3 mol N m^{-2} yr^{-1}) is a factor of 5 larger than the maximum nitrate uptake rate (1.1 mol N m^{-2} yr^{-1}) but almost an order of magnitude larger than the mean uptake rate observed (0.66 mol N m^{-2} yr^{-1}). For comparison, *Naveira-Garabato et al*. [2002] calculated vertical nitrate transport within patches of peak vertical flow in the Antarctic Polar Front (APF) of up to 20% of observed nitrate uptake rates, integrated from the surface to the 0.1% light depth (~50 m). While the findings in *Naveira-Garabato et al*. [2002] indicate that mesoscale vertical advection provides a significant contribution to the nitrate demand in the surveyed region of the APF, the values of local nitrate flux estimated with *wN* in the current study indicate that mesoscale vertical advection as a source of nitrate can locally exceed that required to support the observed biological demand during the D321 survey period.

4.3.2. Nitrate Transport Due to Turbulent Mixing

During cruise D321, turbulence measurements were also made using an ISW microstructure shear turbulence profiler at 21 stations within the survey region over the course of the cruise. The local nitrate flux due to turbulent mixing has been calculated elsewhere [*Forryan et al*., 2012] at each of these stations by using the derived value of k_z (see equation (1)) and in situ nitrate concentrations from discrete bottle samples collected during CTD casts at the same locations as the turbulence measurements. Findings indicate surprisingly little spatial variability in the turbulent nitrate flux across the survey region with an areal mean transport for the base of the euphotic zone of ~0.05 mol N m^{-2} yr^{-1}.

If we consider local nitrate fluxes at the base of the euphotic zone (50 m), the maximum value due to the mesoscale (~1.5 mol N m^{-2} yr^{-1} using *wN*) is approximately 30 times greater in magnitude than the mean transport due to turbulent mixing (0.05 mol N m^{-2} yr^{-1}). The mesoscale net nitrate transport calculated from $<wN>$ (−0.76 mol N m^{-2} yr^{-1}) is an order of magnitude greater than the turbulent transport. However, the sign is reversed; turbulent motion is associated with a net upward transport of nitrate while mesoscale motion is associated with a net downward transport. The comparison is affected by bias, already discussed, in the mesocale transport. Therefore, a comparison of transports is not satisfactory and only local estimates of flux can be reliably compared.

4.3.3. Winter Convection

A crude estimate can be made of deep winter mixing in the region of the current study such that it can be compared with the mesoscale and turbulent transports. Based on regional ARGO float data, the maximum depth of winter mixing in 2007 for the area was found to be ~600 m (http://www.argo.ucsd.edu/index.html). Using the mean nitrate profile from deep (0–1200 m) CTD casts carried out during the survey period, the integrated nitrate concentration above 600 m is ~7000 mmol m^{-2}. If this concentration is distributed evenly over the depth of the winter mixed layer to represent mixing by winter convection, this results in a homogenized concentration of ~12 mmol m^{-3}. This is equivalent to an integrated concentration of 600 mmol m^{-2} above 50 m (depth of the euphotic zone in the current study). If this concentration in the euphotic zone is expressed as an effective transport (as if it had accumulated over the year), this yields a value of nitrate supply to the euphotic zone associated with winter mixing on the order of 0.6 mol N m^{-2} yr^{-1}. For comparison, using a similar approach, *Painter et al*. [2014] estimated this transport to be 0.69 mol N m^{-2} yr^{-1} for this site. This is 1 order of magnitude higher than the in situ measured turbulent nitrate transport, of comparable magnitude but of opposite sign to that estimated for vertical advective transport using $<wN>$ and represents over 90% of the mean nitrate uptake rate of 0.66 mol N m^{-2} yr^{-1}. This estimated value of winter mixing in the Iceland Basin is considerably smaller than previous estimates of up to 1.4 mol N m^{-2} yr^{-1} in the subpolar gyre [*Williams et al*., 2000] based on annual variations in mixed layer depth and climatological mean nitrate profiles [*Conkright et al*., 1994]. This suggests that the current estimate, calculated from the end of summer mean nitrate profile, may be a conservative one and that winter mixing may well be sufficient to account for all the observed nitrate uptake in the euphotic zone observed during cruise D321. Although it is a very different environment, estimates at the summer nitrate-limited BATS time series in the Sargasso Sea indicate that approximately one quarter to one third of the annual nitrate requirement can be supplied by entrainment from the deep ocean to the surface mixed layer, as a result of deep winter convection [*Michaels et al*., 1994]. It should be noted, however, that the BATS estimate is based on a much more accurate quantification of the total annual nitrate supply. Additionally, BATS is nitrate-limited in summer, and both modeling [e.g., *McGillicuddy et al*., 2003] and observational studies [e.g., *Siegel et al*., 1999] have suggested a significant role for year-round mesoscale upwelling in closing the nitrogen budget.

4.3.4. The Submesoscale

In situ and numerical modeling studies have indicated that small-scale frontal (submesoscale) mechanisms may be at least as important for the vertical advection of nutrients as those occurring on the scale of the eddies themselves [*Klein and Lapeyre*, 2009; *Klein et al*., 1998; *Lapeyre and Klein*, 2006; *Legal et al*., 2007; *Levy*, 2008; *Levy et al*., 2001; *Mahadevan and Archer*, 2000]. While both scales of processes have been shown to contribute to the vertical nutrient pump, the question of how they interact and modify the extent to which each other contribute in the real ocean remains largely unanswered (see *Mahadevan* [2015] for a review), partly due to lack of in situ data. Clearly, very high ($<$10 km) horizontal resolution is needed to resolve such small-scale frontal dynamics.

Legal et al. [2007] directly observed and quantified vertical velocities associated with elongated filaments in the strain region between two interacting components of a dipole. Vertical velocity was calculated for three SeaSoar sections orientated perpendicularly to streamlines. The authors made the assumption that variations along track were likely to be considerably larger than those across-track, and a 2-D approximation of the Omega equation was applied to the data in each section. Vertical velocities of 10–20 m d^{-1} were found within filaments of 5–10 km width, alternating between positive (negative) velocities associated with the lighter (denser) water in the filaments. These findings led the authors to highlight the importance of small-scale circulations. The authors hypothesized that additional numerical studies could show that the energetic vertical pump triggered in filaments outside mesoscale eddies may increase the vertical injection of any tracer with a strong vertical gradient, such as nitrate, by a factor of 2 [*Legal et al*., 2007], due to the greater impact of upward flux on nitrate concentration than downward flux, though this makes assumptions about correlations between vertical velocity and nitrate fields that have already been discussed. They did not, however, have sufficient in situ data to test this hypothesis and to quantify the vertical transport of nitrate associated with submesoscale features they identified.

The analysis presented here has demonstrated, like *Legal et al*. [2007], that evidence for vertical motion can be found in frontal regions, here the jet at the center of the dipole. However, as a result of the smoothing necessary to calculate vertical velocities using the Omega equation, small-scale features associated with submesoscale processes are not adequately resolved. Hence, the quantification of the vertical transport could not be extended with any confidence into the submesoscale. However, the high-resolution physical and nitrate data sets collected with the SeaSoar/SUV-6 approach still offer significant potential for examining fine-scale ($<$5 km) vertical injection of nutrients within small-scale fronts and filaments as illustrated by the localized upward transport of water of over 400 m within a patch approximately 5 km in diameter on the periphery of the cyclonic eddy, as discussed in section 3.3.

So while the present study does not directly address the question of whether the submesoscale may be more or less important than the mesoscale for nutrient supply to the upper ocean, it can nevertheless help to shed light on both sets of processes. A valuable extension to the current research could include a two-dimensional analysis of submesoscale vertical velocity along the dogleg section carried out as part of S2. However, the approach taken by *Legal et al*. [2007] would need to be modified to account for variability in jet structure along the axis of the jet as it narrows then widens passing between the two eddies. More generally, estimating typical nitrate transport due to the submesoscale would face similar issues to those discussed in section 4.2.

5. Conclusions

Despite the fact that the importance of the contribution of the mesoscale (and submesoscale) to upper ocean nitrate supply is now well argued from modeling and theoretical perspectives, it has remained poorly quantified by in situ observations due to difficulties in collecting simultaneous hydrographic and nitrate data at the necessary temporal and spatial scales. The use of coincident physical and nitrate data represents a practical step forward in observing and quantifying upper ocean nutrient dynamics associated with the mesoscale. This study has highlighted the need for estimates of nitrate concentration coincident with vertical velocities rather than the use of assumed correlations.

The intention was to gauge the mesoscale vertical transport of nitrate for a typical square of open ocean. The maximum local upward vertical flux of nitrate due to the mesoscale (wN) was found to be 100 times larger than the mean vertical transport due to turbulent mixing. The mesoscale input is also locally in excess of

the maximum observed nitrate uptake rate and a crude proxy for the relative contribution from winter convection. However, the relative significance on a regional scale has been shown to be difficult to estimate largely due to the significant potential bias introduced by nonzero mean vertical velocity. For the latter reason in particular, the question of what is a typical mesoscale transport of nitrate remains open. Until this is solved we will be unable to provide an accurate assessment of the contribution of the mesoscale to the global nitrate supply supporting marine primary production.

Acknowledgments
This work was carried out as part of a PhD studentship supported by the NOC Graduate School of the University of Southampton, the National Oceanography Centre, and the Natural Environment Research Council (NERC). The work was also supported by NERC Oceans 2025 program and National Capability funding. Special thanks also go to the Captain, crew, technical staff, and fellow scientists aboard RRS Discovery during D321. All data are publically available from the British Oceanographic Data Centre (http://www.bodc.ac.uk/). We are grateful to an anonymous referee for their constructive review and specifically for their succinct summary of an implication of our work that was used to frame the hypothesis in the Discussion.

References

Allen, J. T. (2008), *RRS Discovery Cruise 321, 24 Jul-23 Aug 2007. Biophysical Interactions in the Iceland Basin 2007*, 286 pp., National Oceanography Centre Southampton. Southampton, U. K., (National Oceanography Centre Southampton Cruise Report, 23). [Available at http://eprints.soton.ac.uk/50095/.]

Allen, J. T., and D. A. Smeed (1996), Potential vorticity and vertical velocity at the Iceland-Faroes Front, *J. Phys. Oceanogr.*, *26*(12), 2611–2634.

Allen, J. T., D. A. Smeed, A. J. G. Nurser, J. W. Zhang, and M. Rixen (2001), Diagnosis of vertical velocities with the QG omega equation: An examination of the errors due to sampling strategy, *Deep Sea Res., Part I*, *48*(2), 315–346, doi:10.1016/S0967-0637(00)00035-2.

Allen, J. T., et al. (2005), Diatom carbon export enhanced by silicate upwelling in the Northeast Atlantic, *Nature*, *437*(7059), 728–732, doi:10.1038/nature03948.

Boyd, P., A. Pomroy, S. Bury, G. Savidge, and I. Joint (1997), Micro-algal carbon and nitrogen uptake in post-coccolithophore bloom conditions in the northeast Atlantic, July 1991, *Deep Sea Res., Part I*, *44*(9–10), 1497–1517.

Conkright, M. E., S. Levitus, and T. P. Boyer (1994), World Ocean Atlas 1994 Nutrients U.S. Dep. of Commer., National Oceanic and Atmospheric Administration (NOAA), Washington, D. C.

D'Asaro, E., C. Lee, L. Rainville, R. Harcourt, and L. Thomas (2011), Enhanced turbulence and energy dissipation at ocean fronts, *Science*, *332*(6027), 318–322, doi:10.1126/science.1201515.

Falkowski, P. G., D. Zieman, A. H. Knap, and P. K. Bienfang (1991), Role of eddy pumping in enhancing primary production in the ocean, *Nature*, *352*(6330), 55–58.

Finch, M. S., D. J. Hydes, C. H. Clayson, B. Weigl, J. P. Dakin, and T. J. P. Gwilliam (1998), A low power ultraviolet nitrate sensor for use in seawater: Introduction, calibration and initial sea trials, *Anal. Chim. Acta*, *377*, 167–177.

Forryan, A., A. P. Martin, M. A. Srokosz, E. E. Popova, S. C. Painter, and M. C. Stinchcombe (2012), Turbulent nutrient fluxes in the Iceland Basin, *Deep Sea Res., Part I*, *63*, 20–35.

Hoskins, B. J., I. Draghici, and H. C. Davies (1978), A new look at the ω-equation, *Q. J. R. Meteorol. Soc.*, *104*, 31–38.

Jenkins, W. J. (1988), Nitrate flux into the euphotic zone near Bermuda, *Nature*, *331*(6156), 521–523.

Jenkins, W. J., and D. Wallace (1992), Tracer based inferences of new production in the sea, in *Primary Productivity and Biogeochemical Cycles in the Sea*, edited by P. Falkowski and A. Woodhead, Plenum, New York.

Jenkins, W. J., and J. C. Goldman (1985), Seasonal oxygen cycling and primary production in the Sargasso Sea, *J. Mar. Res.*, *43*(2), 465–491.

Jickells, T., et al. (2008), A langrangian biogeochemical study of an eddy in the Northeast Atlantic, *Prog. Oceanogr.*, *76*(3), 366–398.

Klein, P., and G. Lapeyre (2009), The oceanic vertical pump induced by mesoscale and submesoscale turbulence, *Annu. Rev. Mar. Sci.*, *1*, 351–375.

Klein, P., A. M. Treguier, and B. L. Hua (1998), Three-dimensional stirring of thermohaline fronts, *J. Mar. Res.*, *56*(3), 589–612.

Lapeyre, G., and P. Klein (2006), Impact of the small-scale elongated filaments on the oceanic vertical pump, *J. Mar. Res.*, *64*(6), 835–851.

Ledwell, J. R., A. J. Watson, and C. S. Law (1993), Evidence for slow mixing across the pycnocline from an open-ocean tracer-release experiment, *Nature*, *364*(6439), 701–703.

Ledwell, J. R., A. J. Watson, and C. S. Law (1998), Mixing of a tracer in the pycnocline, *J. Geophys. Res.*, *103*(C10), 21,499–21,529, doi:10.1029/98JC01738.

Legal, C., P. Klein, A. Treguier, and J. Paillet (2007), Diagnosis of the vertical motions in a mesoscale stirring region, *J. Phys. Oceanogr.*, *37*(5), 1413–1424.

Levy, M. (2008), The modulation of biological production by oceanic submesoscale turbulence Ocean Sci. Meet., AGU, Orlando.

Levy, M., P. Klein, and A. M. Treguier (2001), Impact of sub-mesoscale physics on production and subduction of phytoplankton in an oligotrophic regime, *J. Mar. Res.*, *59*(4), 535–565.

Lewis, M. R., W. G. Harrison, N. S. Oakey, D. Hebert, and T. Platt (1986), *Vertical Nitrate Fluxes in the Oligotrophic Ocean*, American Association for the Advancement of Science, Washington, D. C.

Mahadevan, A. (2015), Impact of submesoscale physics on primary productivity of plankton, *Annu. Rev. Mar. Sci.*, *8*, 17.1–17.24, doi:10.1146/annurev-marine-010814-015912.

Mahadevan, A., and D. Archer (2000), Modeling the impact of fronts and mesoscale circulation on the nutrient supply and biogeochemistry of the upper ocean, *J. Geophys. Res.*, *105*, 1209–1225, doi:10.1029/1999JC900216.

Martin, A. P., and P. Pondaven (2003), On estimates for the vertical nitrate flux due to eddy pumping, *J. Geophys. Res.*, *108*(C11), 3359, doi:10.1029/2003JC001841.

McGillicuddy, D. J. (2016), Mechanisms of physical-biological-biogeochemical interaction at the oceanic mesoscale, *Annu. Rev. Mar. Sci.*, *8*, 125–159, doi:10.1146/annurev-marine-010814-015606.

McGillicuddy, D. J., and A. R. Robinson (1997), Eddy-induced nutrient supply and new production in the Sargasso Sea, *Deep Sea Res., Part I*, *44*(8), 1427–1450.

McGillicuddy, D. J., A. R. Robinson, D. A. Seigel, H. W. Jannasch, R. Johnson, T. D. Dickey, J. McNeil, A. F. Michaels, and A. H. Knap (1998), Influence of mesoscale eddies on new production in the Sargasso Sea, *Nature*, *394*(6690), 263–265.

McGillicuddy, D. J., R. Johnson, D. A. Siegel, A. F. Michaels, N. R. Bates, and A. H. Knap (1999), Mesoscale variations of biogeochemical properties in the Sargasso Sea, *J. Geophys. Res.*, *104*(C6), 13,381–13,394, doi:10.1029/1999JC900021.

McGillicuddy, D. J., L. A. Anderson, S. C. Doney, and M. E. Maltrud (2003), Eddy-driven sources and sinks of nutrients in the upper ocean: Results from a 0.1degree resolution model of the North Atlantic, *Global Biogeochem. Cycles*, *17*(2), 1035, doi:10.1029/2002GB001987.

McGillicuddy, D. J., et al. (2007), Eddy/wind interactions stimulate extraordinary mid-ocean plankton blooms, *Science*, *316*(5827), 1021–1026.

Michaels, A. F., et al. (1994), Seasonal patterns of ocean biogeochemistry at the U.S. JGOFS Bermuda Atlantic time-series study site International (III), Pergamon, Oxford.

Naveira-Garabato, A. C., J. T. Allen, H. Leach, V. H. Strass, and R. T. Pollard (2001), Mesoscale subduction at the Antarctic Polar Front driven by baroclinic instability, *J. Phys. Oceanogr.*, *31*, 2087–2107.

Naveira-Garabato, A. C., V. H. Strass, and G. Kattner (2002), Fluxes of nutrients in a three-dimensional meander structure of the Antarctic Polar Front, *Deep Sea Res., Part II*, *49*(18), 3771–3792.

Nelson, D. M., and W. O. Smith Jr. (1991), Sverdrup revisited: Critical depths, maximum chlorophyll levels, and the control of Southern Ocean productivity by the irradiance-mixing regime, *Limnol. Oceanogr.*, *36*(8), 1650–1661.

Nielsdóttir, M. C., C. M. Moore, R. Sanders, D. J. Hinz, and E. P. Achterberg (2009), Iron limitation of the postbloom phytoplankton communities in the Iceland Basin, *Global Biogeochem. Cycles*, *23*, GB3001, doi:10.1029/2008GB003410.

Oschlies, A. (2002), Can eddies make ocean deserts bloom?, *Global Biogeochem. Cycles*, *16*(4), 1106, doi:10.1029/2001GB001830.

Painter, S. C., et al. (2014), An assessment of the vertical diffusive flux of iron and other nutrients to the surface waters of the subpolar North Atlantic Ocean, *Biogeosciences*, *11*(8), 2113–2130, doi:10.5194/bg-11-2113-2014.

Pidcock, R. (2011), Quantifying the role of mesoscale-driven processes of nitrate supply within an open ocean eddy dipole doctoral thesis, Univ. of Southampton, Southampton.

Pidcock, R., M. Srokosz, J. Allen, M. Hartman, S. Painter, M. Mowlem, D. Hydes, and A. Martin (2010), A novel integration of an ultraviolet nitrate sensor on board a towed vehicle for mapping open-ocean submesoscale nitrate variability, *J. Atmos. Oceanic Technol.*, *27*(8), 1410–1416.

Pidcock, R., A. Martin, J. Allen, S. C. Painter, and D. Smeed (2013), The spatial variability of vertical velocity in an Iceland basin eddy dipole, *Deep Sea Res., Part I*, *72*, 121–140.

Pollard, R. T., and L. A. Regier (1992), Vorticity and vertical circulation at an ocean front, *J. Phys. Oceanogr.*, *22*(6), 609–625.

Rumyantseva, A., N. Lucas, T. Rippeth, S. Henson, A. P. Martin, and S. C. Painter (2015), Ocean nutrient pathways associated with passage of a storm, *Global Biogeochem. Cycles*, *29*, 1179–1189, doi:10.1002/2015GB005097.

Sambrotto, R. N., J. H. Martin, W. W. Broenkow, C. Carlson, and S. E. Fitzwater (1993), Nitrate utilization in surface waters of the Iceland Basin during spring and summer of 1989, *Deep Sea Res., Part II*, *40*(1-2), 441–457.

Sarmiento, J. L., G. Thiele, R. M. Key, and W. S. Moore (1990), Oxygen and nitrate new production and remineralization in the North Atlantic subtropical gyre, *J. Geophys. Res.*, *95*(C10), 18,303–18,315, doi:10.1029/JC095iC10p18303.

Sévellec, F., A. C. Naveira Garabato, J. A. Brearley, and K. L. Sheen (2015), Vertical flow in the Southern Ocean estimated from individual moorings, *J. Phys. Oceanogr.*, *45*(9), 2209–2220, doi:10.1175/JPO-D-14-0065.1.

Siegel, D. A., D. J. McGillicuddy, and E. A. Fields (1999), Mesoscale eddies, satellite altimetry, and new production in the Sargasso Sea, *J. Geophys. Res.*, *104*(C6), 13,359–13,379, doi:10.1029/1999JC900051.

Spitzer, W. S., and W. J. Jenkins (1989), Rates of vertical mixing, gas exchange and new production: Estimates from seasonal gas cycles in the upper ocean near Bermuda, *J. Mar. Res.*, *47*(1), 169–196.

Thomas, L. N., J. R. Taylor, R. Ferrari, and T. M. Joyce (2013), Symmetric instability in the Gulf Stream, *Deep Sea Res., Part II*, *91*, 96–110, doi:10.1016/j.dsr2.2013.02.025.

Williams, R. G., A. J. McLaren, and M. J. Follows (2000), Interannual variability in the convective and Ekman supply of nitrate to the euphotic zone over the the North Atlantic, *Global Biogeochem. Cycles*, *14*, 1299–1313, doi:10.1029/2000GB001260.

Woods, J. D. (1988), Mesoscale upwelling and primary production, in *Toward a Theory on Biological-Physical Interactions in the World Ocean*, edited by B. J. Rothschild, D. Reidel, Dordrecht, Netherlands.